3D FINITE ELEMENT MODELING OF THE LINEAR FRICTION WELDING OF A BETA TITANIUM ALLOY

W. LI*, Q. YE*, X. WANG*, X. YANG* and T. MA*

** State Key Laboratory of Solidification Processing, Shaanxi Key Laboratory of FrictionWelding Technologies, Northwestern Polytechnical University, Xi'an, 710072, Shaanxi, PR China, liwy@nwpu.edu.cn*

DOI 10.3217/978-3-85125-615-4-28

ABSTRACT

In this study, a 3D numerical model for linear friction welding (LFW) of a metastable beta titanium alloy (Ti-8V-6Cr-4Mo-4Zr-3Al) with a rectangular cross-section was established and validated experimentally. The effects of welding time and oscillatory direction on the thermal profiles, burn-off rates and subsequent microstructures were investigated. The results showed that the interface temperature and width of the weld center zone (WCZ) decreased when the oscillation along the short edge of rectangle compared to that along the long edge. The temperature at the interface was quickly increased to 1000 °C at around 1s; and after 2s, the maximum interface temperature could be over 1052°C and the LFW process reached a quasi-steady state in which the plasticized metal was continuously extruded. With the increase of welding time, the thickness of plasticized layer at the interface decreased, and the grain size in WCZ first increased and then kept stable. The results confirm that the developed model is useful for welding design.

Keywords: linear friction welding; beta titanium alloy; finite element modeling; temperature field; microstructure

INTRODUCTION

Linear friction welding (LFW) is an efficient manufacturing process which allows the solid-state joining or coalescence of non-axisymmetrical metals using frictional heat generated between two rubbing surfaces in a reciprocal motion [1-2]. One of the workpieces is held stationary, and the other one oscillates linearly under compressive forces without external heat and additional welding substance. Once sufficient heat has been generated, the relative movement is stopped and a forging force is applied [3]. The benefits of LFW over conventional welding methods are the absence of solidification defects, the ability of welding dissimilar metallic materials, low consumption, automation, high reproducibility, no production of fumes, short production time, and environmentally friendly [4-5]. It has been applied in very interesting studies of the transportation and especially in aerospace industries. For instance, a very successful application of the LFW process is regard to building up and repairing of aeroengine blisks [6]. As for the LFW process, several

materials are considered, such as steels [7], aluminum alloys [8-9], superalloys [10], titanium alloys [11-12] and so on, but titanium alloys are the most concerned.

LFW is a complicated and strongly thermomechanically coupled physical process, and it is very difficult to study its nature merely by welding experiments. With the development of computer technology and numerical analysis, finite element modeling (FEM) has become a powerful and reliable technique for understanding what is happening during the rapidly evolving process [13-16]. For example, the previously developed models can predict the temperature history [17], stress fields [18], and flash morphology [13] within the welded parts. Different researchers have built two dimensional (2D) or three dimensional (3D) thermomechanically coupled models in Lagrangian or arbitrary Lagrangian–Eulerian (ALE) formulations using an implicit or explicit solver, and commercial softwares like DEFORM [13, 19], ABAQUS [20, 21], ANSYS [17] or FORGE [15] have been used. Grujicic et al. [22] developed the coupled thermo-mechanical 3D model for Ti64 by ABAQUS, with the modified Johnson-Cook material model, and calculated dynamic recrystallization from a custom material subroutine. Although there is some improvement in the temperature field, the size of the mesh is somewhat bulky compared with the workpiece size, so the flash morphology needs to be improved. The majority of the investigations into the LFW process about modeling and experiments were focused on characterizing the process inputs, namely the amplitude, frequency, applied force and burn-off. The effects of the workpiece geometry are often neglected. To the authors' knowledge, only a few journal publications specifically commented on the geometric effects; and most of them used machine data recorded during welding which was post-processed to determine the average heat flux over the initial phase. This was applied to a thermal model to predict the temperature distribution. After this, the single-body method was used to model the equilibrium phase and an inelastic heat fraction was specified to represent the amount of mechanical work converted to heat. Schroerer et al. [19] and McAndrew et al. [13] conducted the fully coupled thermo-mechanical analysis using the single-body modeling approach while applying the plane-strain condition to the 2D model, and experimentally validated 2D models were used to investigate the workpiece geometry effects on the material flow. The 3D model was considered by Sorina-Müller et al. [17] and McAndrew et al. [23], respectively. They provided insight into the effects of the workpiece geometry on the multi-directional material flow behavior of welds. Bilal Ahmad et al. [18] explored the 2D model by ABAQUS to investigate the influence of the oscillation direction on the residual stress.

The present paper reports on the development of a 3D LFW process model for joining Ti-8V-6Cr-4Mo-4Zr-3Al titanium alloy. The purpose of the article is to compare with other results and investigate the reasons why the workpiece geometry affects the process behavior. Some experiments are also carried out to validate the accuracy of the latest version of a process model.

MODELING OF LFW

GEOMETRY AND MESHING

In order to build an efficient control method for LFW, a valid temperature prediction model needs to be established and many basic mechanics of this process need to be understood. The 2D models are unable to express the flash from different direction and temperature field in the welding interface, thus the 3D model of the LFW process tested in this work was created using the software ABAQUS. Samples of the same rectangular cross-section but with two different oscillation directions (along long edge and short edge as shown in Fig. 1a and 1b, respectively), were chosen for the analysis.

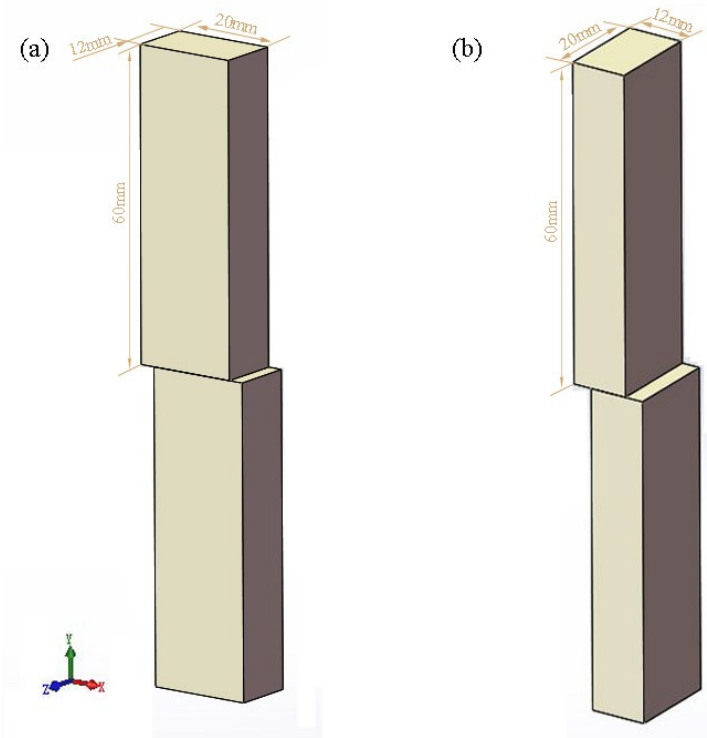

Fig. 1 Workpiece dimensions with different oscillatory lengths: (a) 20mm and (b) 12mm

The detailed 3D model is shown in Fig. 2. Since the deformation and heat flow are considered to be approximately symmetric around the y-plane, only a half of the geometry was included. Instead, a rigid body having the same width as the specimen was used to model the welding interface and the friction process on account of a reasonable compromise between the computation cost and accuracy. The deformed body was divided into two regions, one region of 10mm containing the thermo-mechanically affected zone (TMAZ) and weld center zone (WCZ), therefore characterized by a fine structured mesh (meshing size of approximately 1mm) to predict the temperature accurately and another region of 50 mm with a coarse mesh to reduce the number of elements. The gradient meshes were adopted in TMAZ considering the computation efficiency and accuracy, and the mass scaling factor was set to 20000. The ALE adaptive meshing was adopted in the present paper to maintain a high-quality mesh throughout an analysis, even when large deformations occurred, by allowing the mesh to move independently of the material. The ALE adaptive meshing was used with a remeshing frequency of 1 and remeshing sweeps of 2 per increment. The meshing was conducted using the 8-node brick elements with

coupled displacement and temperature, reduced integration, and hourglass control (C3D8RT) which was based on thermo-mechanical coupling in the LFW process. The total numbers of nodes and elements of the model were 24716 and 22215, respectively.

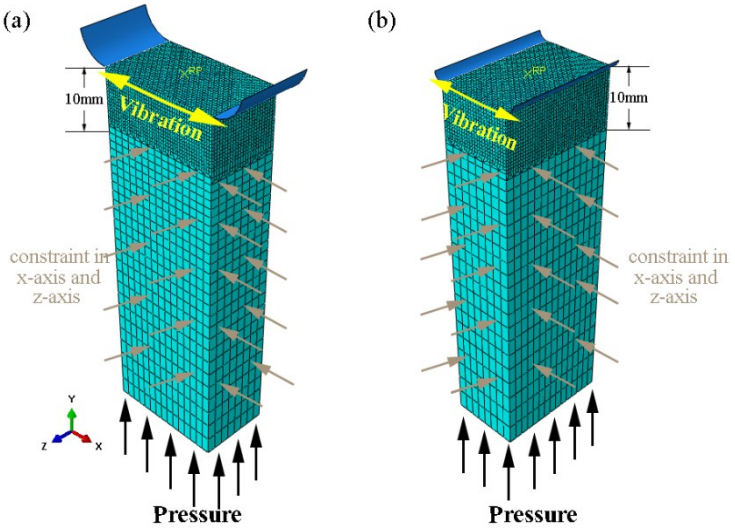

Fig. 2 Sketch of the 3D FEM model under different vibration lengths: (a) 20mm and (b) 12mm

BOUNDARY CONDITIONS

In the initial step, a uniform temperature of 25°C was applied to both samples. The temperature of the environment was also set to 25°C. As shown in Fig. 2, the lower 50mm region was only allowed to move in Y direction while constrained in X and Z directions. The rigid body was only allowed to move in X direction in a sinusoidal mode with a given amplitude and frequency. The type of interaction of the rigid surface and the top surface of the specimen was a surface-to-surface contact. In this study, the thermal radiation and convection coefficients between the workpiece and surroundings were set to 30W/(m^2·°C), and the value of the contact thermal conductance between the workpiece and fixture was 1000W/(m^2·°C). In the LFW process, the primary interaction occurs at the weld interface between workpieces; however, a secondary concern is the possible contact of weld flash with the sides of the body, here it was neglected. The interaction between the workpiece and rigid body was implemented by using the surface-to-surface contact formulation available in ABAQUS.

Due to difficulties in measurement of the friction coefficient, as evidenced by Vairis [24], and lack of available data in the literature, the temperature-dependent values in this study were hypothesized but in a reasonable range dependent on the interface temperature, which is shown in Fig. 3.

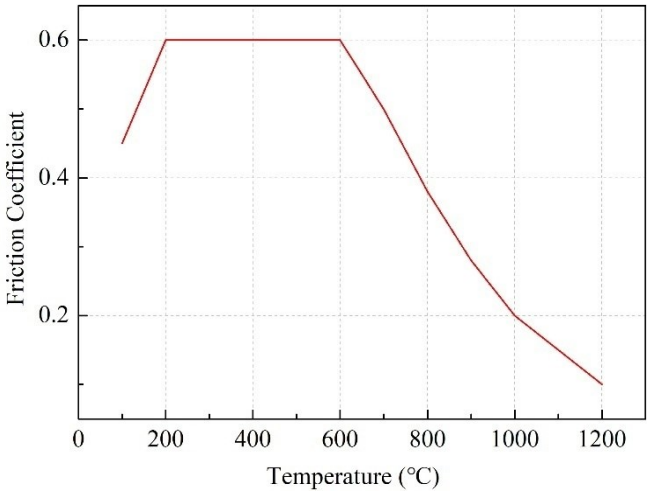

Fig. 3 Temperature dependent friction coefficient of Ti-8V-6Cr-4Mo-4Zr-3Al

One of the important challenges about FEM-based LFW simulations is modeling the weld area because it needs a delicate compromise between accuracy and feasibility. According to Vairis and Frost [25-27], LFW is typically divided into four stages: initial, transition, equilibrium and deceleration (or forging) phases. Since the existing commercial software packages are not capable of joining separate meshes as required for the LFW process, the modeling was carried out for three distinct stages of process, dealing with (i) initial, (ii) transition, and (iii) equilibrium stages [26]. So the applied pressure was applied on the bottom surface of the deformed body during the welding process. The welding parameters, such as friction pressure, oscillation frequency, amplitude and welding time, are listed in Table 1.

Table 1 Selected values for processing parameters

Pressure (MPa)	Frequency (Hz)	Amplitude (mm)	Welding time (s)
70	25	2	4

MATERIAL

The welds were performed on the forged Ti-8V-6Cr-4Mo-4Zr-3Al titanium alloy (nominal chemical composition is given in Table 2). To solve transient thermal problem, it is necessary to define thermal behavior of material; that is identified by specifying thermal conductivity and specific heat as temperature dependent. Since there is no available reports, these material properties were obtained by software JMatPro, as shown in Fig. 4.

Table 2 Nominal chemical composition of Ti-8V-6Cr-4Mo-4Zr-3Al titanium alloy

Al	V	Cr	Mo	Zr	Fe
3.0~4.0	7.5~8.5	5.5~6.5	3.5~4.5	3.5~4.5	≤0.3
Si	C	N	H	O	**Ti**
≤0.10	≤0.05	≤0.03	≤0.015	≤0.12	Bal.

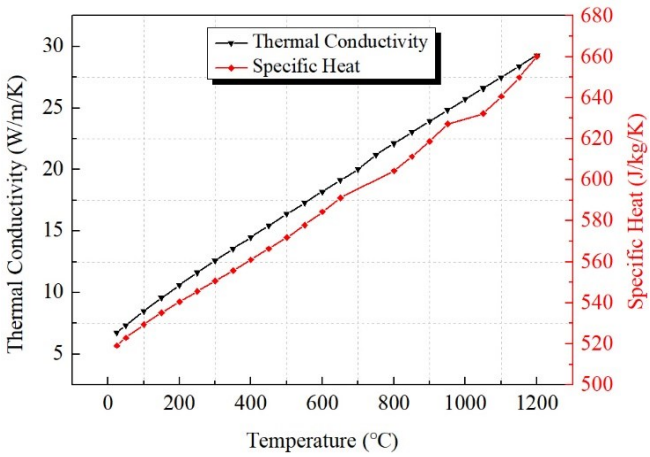

Fig. 4 Thermal conductivity and specific heat of Ti-8V-6Cr-4Mo-4Zr-3Al as temperature dependent

The constitutive behavior of materials is usually expressed by a nonlinear equation, which is a relationship among flow stress, strain, strain rate and temperature. The inelastic behavior of the investigated alloy is assumed to be described by Johnson–Cook (JC) constitutive material model as follows [28]

$$\sigma = \left(A + B\varepsilon_p^n\right)[1 + Cln(\dot{\varepsilon}^*)][1 - (T^*)^m] \quad (1)$$

where σ is the flow stress. A and B are the strain hardening parameters; C is a dimensionless strain rate strengthening coefficient; n and m are power exponents of the strain hardening and thermal softening terms; ε_p is the effective plastic strain. $\dot{\varepsilon}^*$ is calculated by the expression $\dot{\varepsilon}^* = \dot{\varepsilon}_p/\dot{\varepsilon}_0$. $\dot{\varepsilon}_p$ is the effective plastic strain rate. $\dot{\varepsilon}_0$ is the reference plastic strain rate. $\dot{\varepsilon}_0$ is normally selected as 1 S^{-1}. T^* is a homologous temperature, which is expressed by the expression $T^* = (T - T_r)/(T_m - T_r)$. T_r and T_m are the reference temperature and the melting point, respectively. The room temperature was set as 25°C. The melting temperature was set as 1220°C. The JC material model parameters for Ti-8V-6Cr-4Mo-4Zr-3Al (A = 436.14 MPa, B = 90 MPa, n = 0.48, C = 0.552, m = 1.05, $\dot{\varepsilon}_0$ = 1 S^{-1}) were taken from our previous research for hot deformation behaviors.

EXPERIMENTAL PROCEDURE

The experimental Ti-8V-6Cr-4Mo-4Zr-3Al workpieces dimensions used in this study are also displayed in Fig. 1. It is a kind of metastable beta titanium alloy, which consists of equiaxed beta grains, as shown in Fig. 5. The welding equipment used was the XMH-250 LFW machine developed in house by Northwestern Polytechnical University. The experimental conditions investigated in this work are displayed in Table 1. To investigate the correlation between microstructure change and temperature field during LFW, the LFW machine was stopped during the process cycle at specified times (1, 2 and 4 s) for the dimension of 20mm×12mm×60mm.

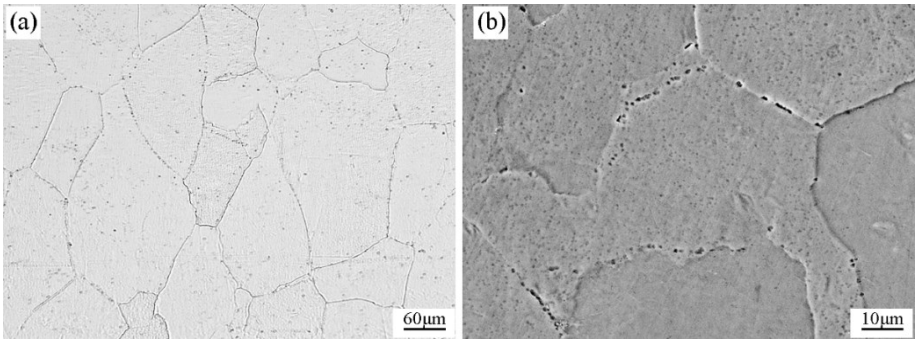

Fig. 5 Microstructure of the Ti-8V-6Cr-4Mo-4Zr-3Al base metal: (a) OM and (b) SEM

Metallographic specimens were produced from the experiments, and they were sectioned and polished so that the center of the weld may be viewed in-plane to the direction of oscillation. The sectioned samples were mounted and then ground using 600, 1000, 2000 and 3000 silicon carbide grit papers. After grinding, the sectioned samples were polished using colloidal silica on a micro-cloth and etched using a solvent of 0.5 mL HF, 1.5 mL HNO_3, 2 mL HCl and 96 mL distilled water. The metallographic samples were viewed under the optical microscope (OM) (OLYMPUS PMG3) to investigate the microstructure.

RESULT AND DISCUSSION

MODEL VERIFICATION

Fig. 6 shows the comparisons between simulated and experimental burn-off. It can be seen that there are some deviations between the experimental axial shortening values and simulation results. The changing trend of the two curves is consistent basically. The computed burn-off generally deviates less than 5% (in some rare instances up to 15%) from the experiment. The initial time that the two samples came into contact with each other is difficult to determine because the workpieces are not smooth entirely in the fact, but initial phase is neglected in the simulation. Therefore, burn-off increases persistently in the dash line curve.

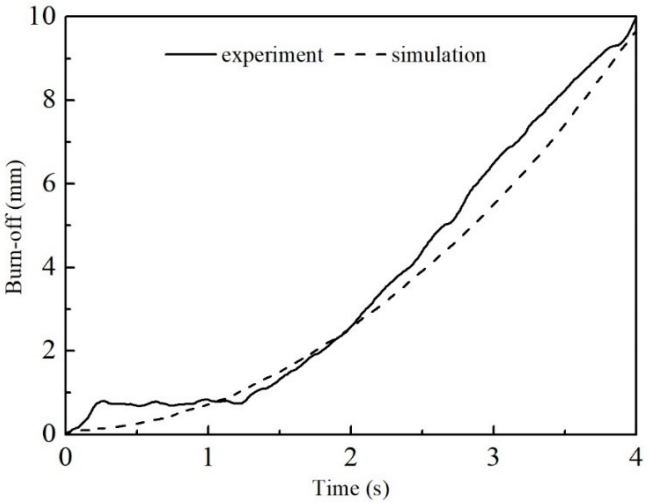

Fig. 6 Calculated and experimental burn-off as a function of process time for 20mm of oscillatory direction

The result shows that the numerical model and the calculation method for deformation of material are proper and could be applied in further investigations.

TEMPERATURE FIELD

All simulations are carried out with the same initial and boundary conditions. Typical temperature distributions are shown in Fig. 7. When the welding process is finished, the interface is covered by high temperature metal, and flash is cooler than the interface. Fig. 8 shows the temperature distribution at the center vertical to the y axis. For an identical combination of process inputs, the models shows that the extent of the TMAZ decreases when the workpieces are oscillated along the shorter of the two interface contact dimensions, i.e. the 12mm dimension. This is because the material farther back from the interface was is much cooler in this weld. When this cooler material reaches the weld interface, it effectively cools the weld, producing a lower interface temperature (Fig.7), which is in agreement with the results of McAndrew et al. [13] and Schroeder et al. [19].

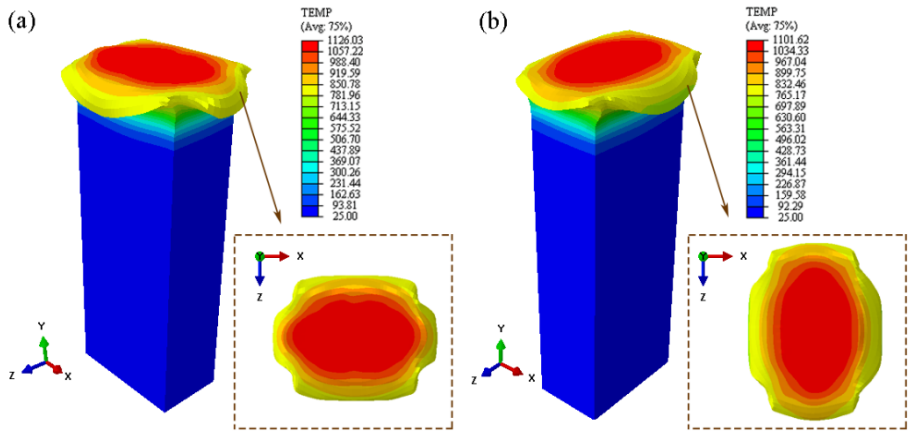

Fig. 7 Temperature distribution in the rubbing interface when welding is finished: (a) the oscillation in the 20mm edge and (b) the oscillation in the 12mm edge

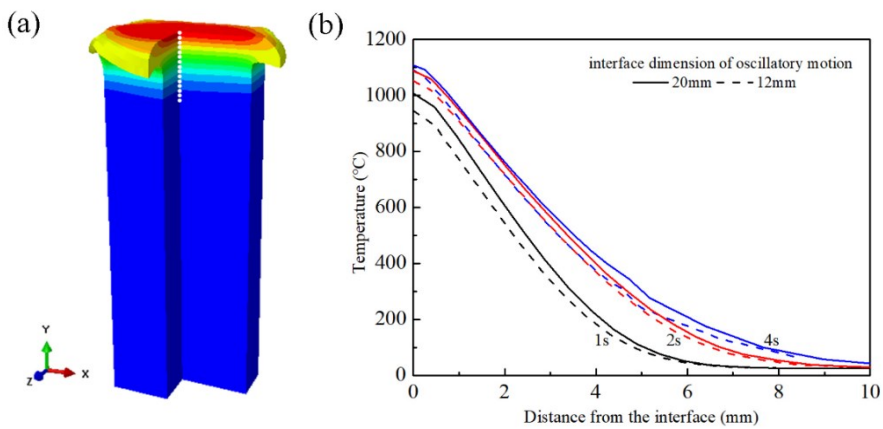

Fig. 8 Thermal gradient recorded from the model: (a) data output from the model middle and (b) the temperature gradient at different welding times

The calculated temperature evolution at the center point is shown in Fig. 9. The temperature of interface center rises to 1000℃ within 1s rapidly, and after 2s, the maximum interface temperature could be over 1050°C. For the long oscillatory length, i.e. 20mm, the temperature rises more rapidly at first, temperature rise rate is larger, and the time to reach the quasi-steady state is shorter. This is because that when a certain amplitude is applied, the long oscillatory length has less un-contact area between two workpieces, which leads to effective heat input increased, and interface temperature rises faster. Under the chosen welding conditions and geometries, it can be concluded from the calculations that no liquid phase exists during the welding process.

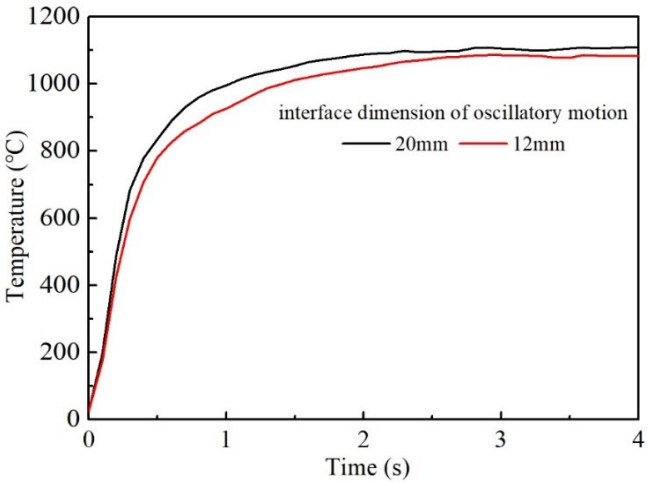

Fig. 9 The calculated temperature evolution in the interface under two oscillation directions

BURN-OFF HISTORY

The time-dependent burn-off processes are shown in Fig. 10. Within the beginning 1.5 s, the burn-off is very small, the reason is that during this period, welding has not reached the quasi-steady state, and the temperature distribution of the interface is non-uniform, thus a few high temperature material cannot be expelled sufficiently. As friction continuing, the quasi-steady state is reached, thus the plasticity of interface material increases, then a layer of plastic metal at interface generates. Accordingly, the high-temperature plastic metal of the interface is extruded continuously to form flash, leading to burn-off to increase gradually. The burn-off rate is affected by the oscillatory length. Decreasing the oscillatory length of the workpiece caused the burn-off rate to increase, because the material at the WCZ has to be transported further to be extruded in the oscillation direction, and a reduction of the vibratory width removes a higher percentage of the total interface material with each cycle of oscillation before the steady state.

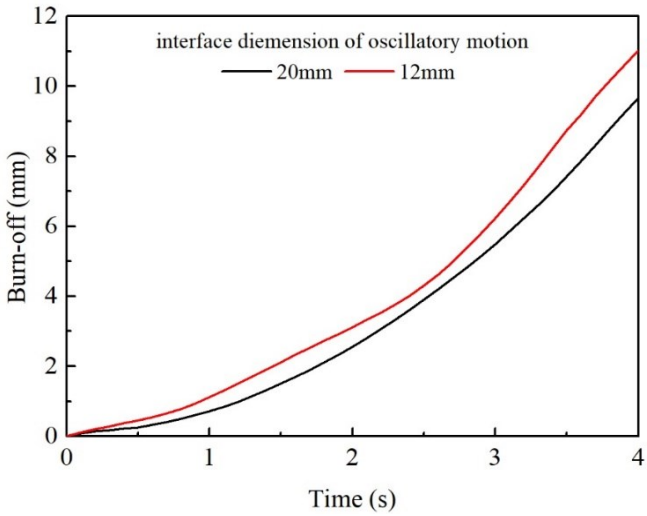

Fig. 10 Calculated axial shortening (burn-off) for different oscillatory lengths

MICROSTRUCTURE ANALYSIS

The typical microstructures of LFWed Ti-8V-6Cr-4Mo-4Zr-3Al joint is shown in Fig. 11. There are fine equiaxed β phase grains in the WCZ (see Fig. 11b) with a size of 10-20μm, and the structure is not continuous. The welding process is characterized by severe plastic deformation, followed by fast cooling to room temperature. Moreover, the dynamic recrystallization can occur under the high temperature and the deformation, but short heating time restricts the grain growth. Further away from the weld line (starting from about 80μm, Fig. 11c), the microstructure shows evidence of severe plastic deformation during the welding process on both sides of the weld line, which is called TMAZ. The original grains are deformed heavily and re-oriented during the welding process in the direction of the friction motion and thus along the direction of material flow. The microstructure in the WCZ is different from that of the biphasic titanium alloy like Ti-6Al-4V, where is no martensite [29]. As α phase is little, only dynamic recrystallization occurs without phase transformation, and the microstructure is similar to that of the high-temperature superalloy [30].

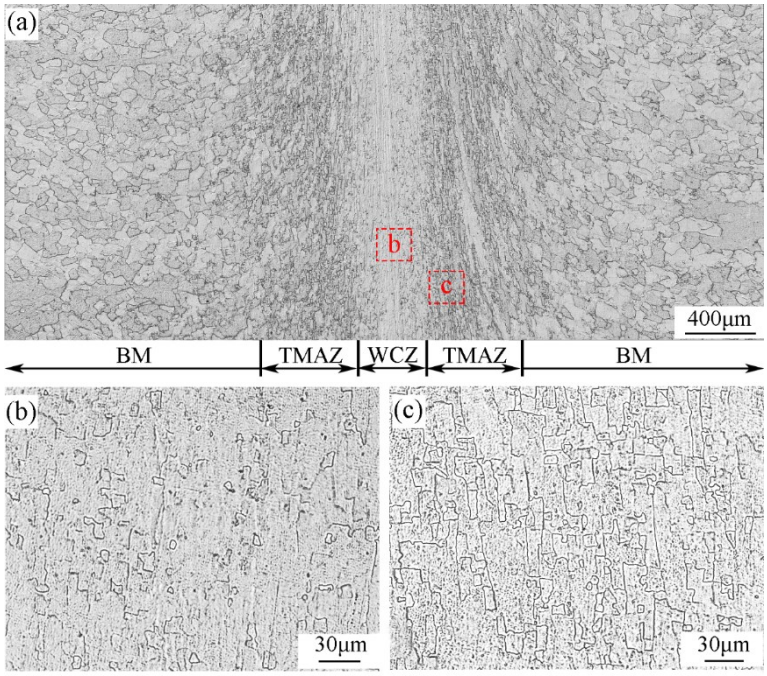

Fig. 11 Typical microstructure of the LFWed Ti-8V-6Cr-4Mo-4Zr-3Al joint: (a) microstructure vertical to oscillatory direction, (b) high magnification of WCZ and (c) TMAZ

The cross-sectional microstructures under different welding times along the 20mm-oscillatory direction are shown in Fig. 12. When the welding time is 1s, the width of the WCZ is 555μm. As the welding goes on (about 2s), the width begins to decrease (233μm), and finally the width tends to be stable (246μm). Because the friction time is short, high-temperature region is small (Fig. 8), and heat input is insufficient to make thermoplastic metal cover the interface completely, thus only parts of the interface have been combined (see Fig. 12a), and a few of flash has been extruded. The accumulated heat is not taken away through the small flash, and could only be conducted along the vertical direction of the interface to the base metal. Therefore, the width of this weld is wider. As friction goes on, the welding process turns into the equilibrium stage, because heat accumulates progressively, thermoplastic metal of the interface continues to increase, then covers the entire interface completely, and is expelled from the interface to form a continuous, closed flash, finally, the width of welds decreases (see Fig. 12b). After the equilibrium stage is reached, the amount of the flash tends to be stable, and the WCZ width does not change, just like Fig. 12c.

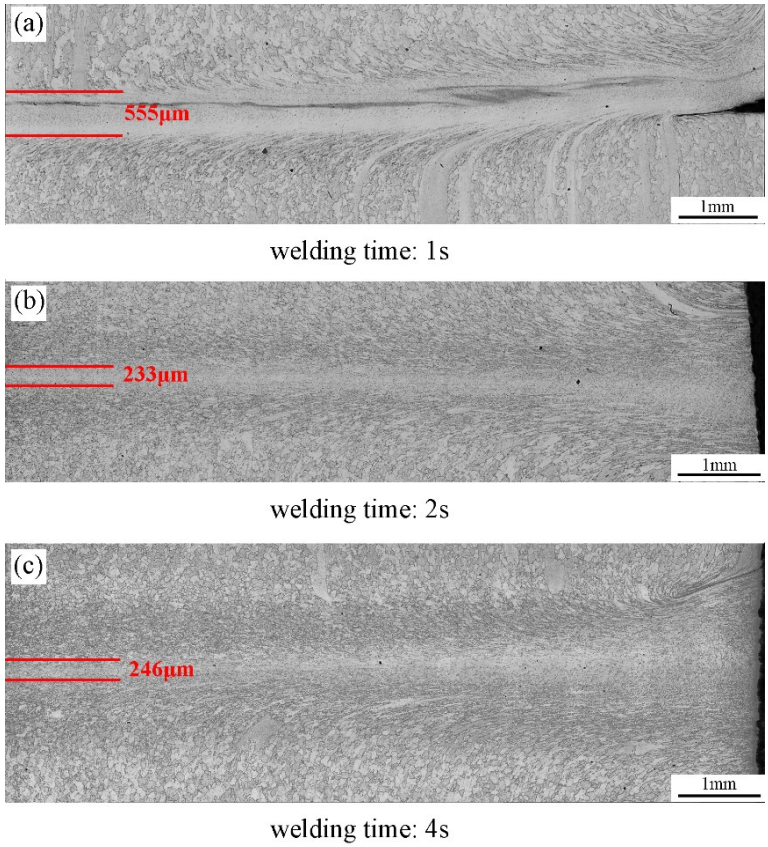

Fig. 12 Overall views of linear friction welded Ti-8V-6Cr-4Mo-4Zr-3Al joints at different friction times: (a) 1s, (b) 2s, and (c) 4s

Fig. 13 is the microstructure of WCZ for different oscillatory directions. It figures that for the same combination of process inputs, the width of the WCZ appeared much narrower (about 200μm) that is produced with smaller oscillatory width (compare Fig. 13a and 13b), which is in agreement with Karadge et al. [9]. And the experimental values are consistent with the models (Fig. 8). The smaller oscillatory width has a greater burn-off rate, so the temperature gradient vertical to the friction direction is greater, and the deformed area is smaller.

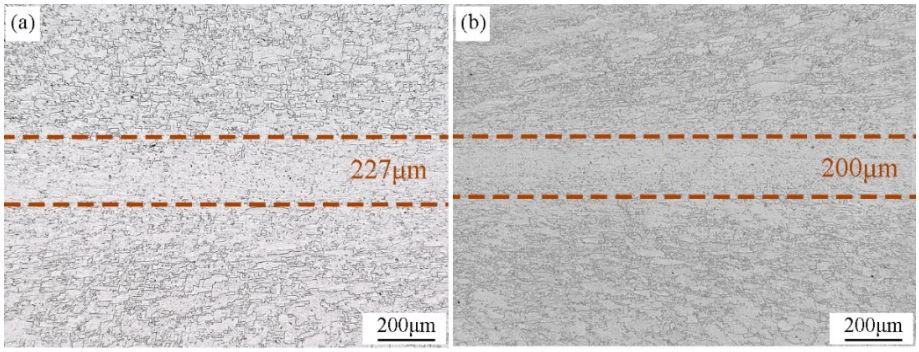

Fig. 13 Experimental WCZ for: (a) the oscillation in the 20mm edge and (b) the oscillation in the 12mm edge

CONCLUSIONS

The primary conclusions from this work are as follows:

- The 3D model predicts fairly well the LFW process compared to experimental results for the conditions investigated here.
- During the LFW process, the temperature in WCZ rises rapidly within 1s to about 1000 °C, high temperature area mainly concentrates in the center of interface. With welding continuing, high temperature area increases further, a large amount of the plastic metal is extruded to form larger flash. There are fine β phase grains instead of martensite in the WCZ.
- A reduction of the oscillatory width increases the steady-state burn-off rate. Furthermore, a reduction of the oscillatory width decreases the interface temperature, but increases the burn-off.
- Burn-off increases with the extension of the friction time, but the plastic metal layer thickness decreases at first and tends to be stable finally.

ACKNOWLEDGEMENTS

The authors would like to acknowledge the financial support from the National Natural Science Foundation of China (No. 51675435). The project was supported by the fund of Key research and development plan (No.2016YFB1100104).

REFERENCES

[1] I. BHAMJI, M. PREUSS, P. L. THREADGILL, A. C. ADDISON: 'Solid state joining of metals by linear friction welding: a literature review', *Materials Science & Technology*, Vol. 27, No. 1, pp. 2-12, 2011.

[2] A. MATEO: 'On the feasibility of blisk produced by linear friction welding', *Revista De Metalurgia*, Vol. 50, No. 3, pp. e023, 2014.

[3] A. R. MCANDREW, P. A. COLEGROVE, C. BÜHR, B. C. D. FLIPO, A. VAIRIS: 'A literature review of ti-6al-4v linear friction welding', *Progress in Materials Science*, Vol. 92, pp. 225-257, 2018.
[4] J. L. HUANG, N. WARNKEN, J. C. GEBELIN, M. STRANGWOOD, R. C. REED: 'On the mechanism of porosity formation during welding of titanium alloys', *Acta Materialia*, Vol. 60, No. 6-7, pp. 3215-3225, 2012.
[5] C. PANWISAWAS, B. PERUMAL, R. M. WARD, N. TURNER, R. P. TURNER, J. W. BROOKS, H. C. BASOALTO: 'Keyhole formation and thermal fluid flow-induced porosity during laser fusion welding in titanium alloys: experimental and modelling', *Acta Materialia*, Vol. 126, pp. 251-263, 2016.
[6] Y. GUO, T. JUNG, L. C. YU, H. LI, S. BRAY, P. BOWEN: 'Microstructure and microhardness of ti6246 linear friction weld', *Materials Science & Engineering A*, Vol. 562, No. 1, pp. 17-24, 2013.
[7] T. J. MA, W. Y. LI, Q. Z. XU, Y. ZHANG, J. L. LI, S. Q. YANG, H, L. LIAO: 'Microstructure evolution and mechanical properties of linear friction welded 45 steel joint', *Advanced Engineering Materials*, Vol. 9, No. 8, pp. 703-707, 2010.
[8] H. MOGAMI, T. MATSUDA, T. SANO, R. YOSHIDA, H. HORI, A. HIROSE: 'High-frequency linear friction welding of aluminum alloys', *Materials & Design*, Vol. 139, pp. 457-466, 2018.
[9] G. BUFFA, M. CAMMALLERI, D. CAMPANELLA, U. L. COMMARE, L. FRATINI: 'Linear friction welding of dissimilar AA6082 and AA2011 aluminum alloys: microstructural characterization and design guidelines', *International Journal of Material Forming*, Vol. 10, No. 3, pp. 307-315, 2017.
[10] T. J. MA, X. CHEN, W. Y. LI, X. W. YANG, Y. ZHANG, S. Q. YANG: 'Microstructure and mechanical property of linear friction welded nickel-based superalloy joint', *Materials & Design*, Vol. 89, pp. 85-93, 2016.
[11] X. Y. WANG, W. Y. LI, T. J. MA, A. VAIRIS: 'Characterisation studies of linear friction welded titanium joints', *Materials & Design*, Vol. 116, pp. 115-126, 2017.
[12] Y. GUO, M. M. ATTALLAH, Y. CHIU, H. LI, S. BRAY, P. BOWEN: 'Spatial variation of microtexture in linear friction welded Ti-6Al-4V', *Materials Characterization*, Vol. 127, pp. 342-347, 2017.
[13] A. R. MCANDREW, P. A. COLEGROVE, A. C. ADDISON, B. C. D. FLIPO, M. J. RUSSELL, L. A. LEE: 'Modelling of the workpiece geometry effects on Ti–6Al–4V linear friction welds', *Materials & Design*, Vol. 87, No. 1, pp. 1087-1099, 2015.
[14] P. S. EFFERTZ, F. FUCHS, N. ENZINGER: 'The influence of process parameters in linear friction welded 30CrNiMo8 small cross-section: a modelling approach', *Science and Technology of Welding and Joining*, (Published online), 2018.
[15] R. TURNER, J. C. GEBELIN, R. M. WARD, R. C. REED: 'Linear friction welding of Ti–6Al–4V: modelling and validation', *Acta Materialia*, Vol. 59, No.10, pp. 3792-3803, 2011.
[16] P. JEDRASIAK, H. R. SHERCLIFF, A. R. MCANDREW, P. A. COLEGROVE: 'Thermal modelling of linear friction welding', *Materials & Design*, Vol.156, pp.362-369, 2018.
[17] J. SORINA-MÜLLER, M. RETTENMAYR, D. SCHNEEFELD, O. RODER, W. FRIED: 'FEM simulation of the linear friction welding of titanium alloys', *Computational Materials Science*, Vol. 48, No. 4, pp. 749-758, 2010.
[18] C. BÜHR, B. AHMAD, P. A. COLEGROVE, A. R. MCANDREW, H. GUO, X. ZHANG: 'Prediction of residual stress within linear friction welds using a computationally efficient modelling approach', *Materials & Design*, Vol. 139, pp. 222-233, 2018.
[19] F. SCHROEDER, R. M. WARD, R. P. TURNER, A. R. WALPOLE, M. M. ATTALLAH, J. C. GEBELIN, R. C. REED: 'Validation of a model of linear friction welding of ti6al4v by considering welds of different sizes', *Metallurgical & Materials Transactions B*, Vol. 46, No. 5, pp. 2326-2331, 2015.

[20] W. LI, F. WANG, S. SHI, T. MA, J. LI, A. VAIRIS: '3D finite element analysis of the effect of process parameters on linear friction welding of mild steel', *Journal of Materials Engineering & Performance*, Vol. 23, No. 11, pp. 4010-4018, 2014.
[21] W. LI, J. GUO, X. YANG, T. MA, A. VAIRIS: 'The effect of micro-swinging on joint formation in linear friction welding', *Journal of Engineering Science & Technology Review*, Vol. 7, No. 5, pp. 55-58, 2014.
[22] M. GRUJICIC, G. ARAKERE, B. PANDURANGAN, C. F. YEN, B. A. CHEESEMAN: 'Process modeling of Ti-6Al-4V linear friction welding (LFW)', *Journal of Materials Engineering & Performance*, Vol. 21, No. 10, pp. 2011-2023, 2012.
[23] A. R. MCANDREW, P. A. COLEGROVE, B. C. D. FLIPO, C. BÜHR: '3D modelling of Ti–6Al–4V linear friction welds', *Science and Technology of Welding and Joining*, Vol. 22, pp. 496-504, 2016.
[24] A. VAIRIS: 'Investigation of frictional behaviour of various materials under sliding conditions', *European Journal of Mechanics - A/Solids*, Vol. 16, No. 6, pp. 929-945, 1997.
[25] A. VAIRIS, M. FROST: 'On the extrusion stage of linear friction welding of Ti6Al4V', *Materials Science & Engineering A*, Vol. 271, No. 1–2, pp. 477-484, 1999.
[26] A. VAIRIS, M. FROST: 'High frequency linear friction welding of a titanium alloy', *Wear*, Vol. 217, No. 1, pp. 117-131, 1998.
[27] A. VAIRIS, M. FROST: 'Modelling the linear friction welding of titanium blocks', *Materials Science & Engineering A*, Vol. 292, No. 1, pp. 8-17, 2000.
[28] G. R. JOHNSON, W. H. COOK: 'A constitutive model and data for metals subjected to large strains, high strain rates and high temperatures', *Proceedings of Seventh International Symposium on Ballistics*, The Hague, pp. 541-547, 1983.
[29] Y. GUO, M. M. ATTALLAH, Y. CHIUA, H. LI, S. BRAY, P. BOWENA. 'Spatial variation of microtexture in linear friction welded Ti-6Al-4V', *Materials Characterization*, Vol. 127, No. 1, pp. 342-347, 2017.
[30] X YANG,W LI, J LI, B XIAO, T MA, Z HUANG, J Guo. 'Finite element modeling of the linear friction welding of GH4169 superalloy', *Materials and Design*, Vol. 87, No. 1, pp. 215-230, 2015.